Physiologically Oriented Models of the Hemodynamic Response in Functional MRI

Frithjof Kruggel and D. Yves von Cramon

Max-Planck-Institute of Cognitive Neuroscience,
Stephanstraße 1, 04103 Leipzig, Germany
{kruggel, cramon}@cns.mpg.de

Abstract. Today, most studies of cognitive processes using functional MRI (fMRI) experiments adopt highly flexible stimulation designs, where not only the activation amount but also the time course of the measured hemodynamic response is of interest. The measured signal only indirectly reflects the underlying neuronal activation, and is understood as being convolved with a hemodynamic modulation function. An approach to better allow inferences about the neuronal activation is given by modeling this convolution process. In this study, we investigate this approach and discuss computational models for the hemodynamic response. An analysis of a recent fMRI experiment underlines the usefulness of this approach.

1 Introduction

Functional magnetic resonance imaging (fMRI) has become one of the major experimental methods for analyzing cognitive processes in humans. The most common fMRI technique employs the blood-oxygen-level-dependent (BOLD) contrast [1], which is sensitive to changes of the relative local concentration of oxygenated hemoglobin (HbO_2) vs. deoxy-hemoglobin and thus reflects an indirect measure of the brain's neuronal activation. This effect is small, and data are noisy: thus, analysis of fMRI data has mostly focused on the detection and statistical quantification of functional activation.

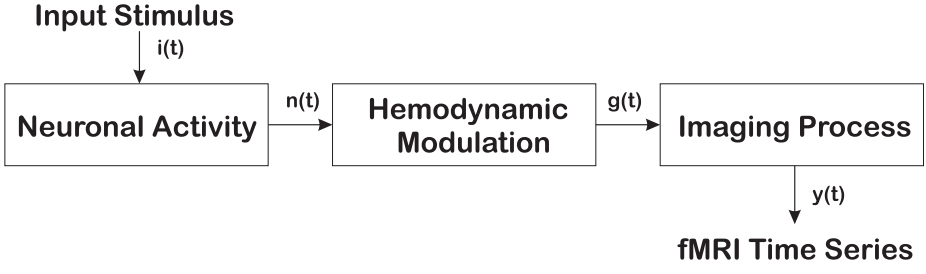

Fig. 1. Signals at various stages of the convolution model of fMRI time series

A. Kuba et al. (Eds.): IPMI'99, LNCS 1613, pp. 294–307, 1999.

Understanding brain function requires information not only on the spatial localization of neural activity, but also on its temporal evolution. There is an increasing interest in the time course (i.e. the shape) of the hemodynamic response (HR) and its modulation with respect to different experimental conditions. The measured fMRI signal $y(t)$ is understood as the result from a series of convolutions of the input stimulus function $i(t)$ ([2], see Fig. 1). So the question was raised to what extent conclusions may be drawn about the neuronal activation $n(t)$ from the HR shape $g(t)$. For example, the hemodynamic modulation introduces time constants at least an order longer than the underlying functional activation; the time-to-maximum of a HR due to a transient stimulus is typically delayed by 5-8s and dispersed by 3-4s [3]. So the key to detecting changes in the neuronal activation is the adoption and deconvolution of the HR by a model function [4].

A number of heuristic functions have been proposed to describe the hemodynamic response: the Poisson function [3], the Gamma function [5,6], a linear combination of the Gamma function and its temporal derivatives [7], and the Gaussian function [8]. The evolution of these approaches follows their modeling complexity; early approaches assumed constant pre-set values for the lag [3], while current models determined HR parameters voxelwise in the time series [5,6,8], or even per stimulus period [9]. HR parameters were shown to depend on the subject, the site and the stimulation conditions [8,9,10], which underlines the usefulness of this approach. However, some issues were raised.

- With the Poisson or the Gamma functions, interesting shape characteristics like delay (time-to-maximum), rise and fall times are hard to obtain.
- While the best fits to an HR are generally found with the Gaussian function, especially responses following short stimuli were asymmetric (shorter rise than fall times).
- For a better understanding of the underlying neuronal processes, a deconvolution of the hemodynamic modulation to yield parameters of the neuronal activation directly is highly desirable.
- None of these functions is based on a physiological model. Although models of the oxygen delivery at membranes have been proposed [11], details of the neurono-vascular coupling are still under discussion and have not yet led to a comprehensive physiological model of hemodynamic modulation.

Aims of this study were: (1) to test the feasibility of introducing more complex model functions for the HR, (2) to separate parameters describing the hemodynamic modulation from parameters of neuronal activation, and (3) to find physiologically more plausible models for the hemodynamic modulation.

Recently, we described and validated a non-linear regression context [9] to model the HR per stimulation period (trial) and region-of-interest (ROI), which is briefly reviewed in the next section, along with a discussion of the three model functions studied here: (1) the Gaussian function, (2) a convolved asymmetric Gaussian function, and (3) a convolved compartment model. To compare the usefulness of these approaches, we re-analyzed a fMRI study of working memory.

2 Description of the Estimation Model

A theoretical discussion and validation of our estimation model is described elsewhere [9]. For an excellent discussion about non-linear regression procedures, see [12]. Throughout this paper, we assume that the locus of a functional activation is known. This knowledge may arise from a previous determination by well-established signal detection procedures or defined as regions of neurofunctional interest. These regions are considered as stationary in space. Note that we focus on single trial experimental designs here: a single cognitive task is given, and the hemodynamic response to this stimulus recorded.

2.1 Model Definition

We consider a subset of the fMRI data collected spatially from a ROI of k voxels and temporally from a single experimental trial at l discrete timesteps and denote this $n = k * l$-dimensional vector as $\mathbf{y}$. Timesteps are referenced by a l-dimensional vector $\mathbf{t}$. We model the hemodynamic response as a deterministic function $g(\mathbf{t}, \boldsymbol{\beta})$, where $\boldsymbol{\beta}$ denotes a p-dimensional vector of model parameters, and we require that $g(\mathbf{t}, \boldsymbol{\beta})$ is differentiable at least once with respect to $\boldsymbol{\beta}$. Data $\mathbf{y}$ are composed of $g(\cdot)$ and a stochastic part $\boldsymbol{\epsilon}$:

$$\mathbf{y} = g(\mathbf{t}, \boldsymbol{\beta}) + \boldsymbol{\epsilon}. \tag{1}$$

The stochastic part is independent of the signal and stationary with respect to time, and its elements are normally distributed with a nonsingular covariance matrix $\mathbf{V}$:

$$\boldsymbol{\epsilon} \sim N_n(0, \mathbf{V}), \qquad \text{then} \qquad \mathbf{y} \sim N_n(g(\boldsymbol{\beta}), \mathbf{V}). \tag{2}$$

This allows us to use preprocessed data where the processing has introduced (or enhanced) a correlation structure. A way to determine the covariance structure from experimental data is described later in this section.

We will now propose the model functions $g(\cdot)$ investigated in this paper. The first two are heuristic but offer a parsimonous number of parameters. The third function is complex but tries to incorporate the properties of tissue compartments involved in the BOLD effect.

Model 1: Gaussian Function The best compromise between goodness-of-fit and the number of model parameters is found with the Gaussian function [8]:

$$g(t, \boldsymbol{\beta}) = a \exp(-(t - t_0)^2 / (2d_0^2)) + b. \tag{3}$$

We denote the 4 components of $\boldsymbol{\beta}$ as a: gain (the "height" of the HR), d_0: dispersion (proportional to the duration of the HR), t_0: lag (the time from stimulation onset to the HR peak), and b: baseline. Here, no distinction can be made between "neuronal" and "vascular" parameters.

Model 2: Convolved Asymmetric Gaussian Function A first approach to closer model the processes depicted in Fig. 1 is to define the HR function $g(t)$ by a convolution of a neuronal stimulation function $n(t)$ with a hemodynamic modulation function $f(t)$:

$$g(t, \boldsymbol{\beta}) = n(t) \otimes f(t) + b, \tag{4}$$

where $\otimes$ denotes the convolution operator and b is a baseline term. We simply assume a square-wave function for the neuronal stimulation $n(t)$:

$$n(t) = \begin{cases} a \text{ if } t >= t_0 \text{ and } t < t_0 + t_1, \\ 0 \text{ otherwise.} \end{cases} \tag{5}$$

A Gaussian function is introduced for hemodynamic modulation function $f(\cdot)$, here with different dispersions (d_0, d_1) for the rising and the falling edge:

$$f(t) = \begin{cases} \exp(-t^2/(2d_0^2)) \text{ if } t < 0, \\ \exp(-t^2/(2d_1^2)) \text{ if } t >= 0. \end{cases} \tag{6}$$

In this model, $\boldsymbol{\beta}$ consists of 6 parameters (d_0: dispersion on the rising edge, d_1: dispersion on the falling edge, a: gain, t_0: neuronal response onset, t_1: neuronal response duration, b: offset). Modeling of the convolution process allows us to address the meaning of a, t_0, and t_1 as "neuronal" parameters, resp. d_0, d_1 as vascular parameters.

Model 3: Convolved Compartment Model In model 3, the formulation of a stepwise defined Gaussian function for the hemodynamic modulation function $f(\cdot)$ is still heuristic. It is physiologically more plausible to model the hemodynamic modulation process by a compartment model. We define the HR model function $g(t)$ as in 4 and the neuronal stimulation $n(t)$ as in 5 and now focus on a new definition of $f(t)$.

For the BOLD contrast, as discussed in the introduction, it is viable to think of the oxygenated blood as an "endogenous tracer" of brain activation. The kinetic of external tracers such as radioactive markers or pharmaceuticals have successfully been modeled by compartment models since 1920 [13]. This modeling context is rich and well understood (for introductions, see [12,14]). Compartments correspond to a body subspaces (i.e. tissue, vasculature), in which the local concentration of a tracer (i.e. oxygenated blood) is modified by transport between compartments (i.e. by diffusion, flow) or active processes (i.e. by consumption). If we assume a linear imaging process, then the HR measured in fMRI is proportional to the HbO_2 concentration, and a compartment model should allow us to draw conclusions about the temporal oxygen flow pattern. Such a model is depicted in Fig. 2.

HbO_2 flows from the arterial into the capillary compartment at a rate γ_0, as mediated by a consumption process in the tissue compartment. The oxygen exchange between capillaries and tissue is described by rates γ_1 and γ_2. Finally,

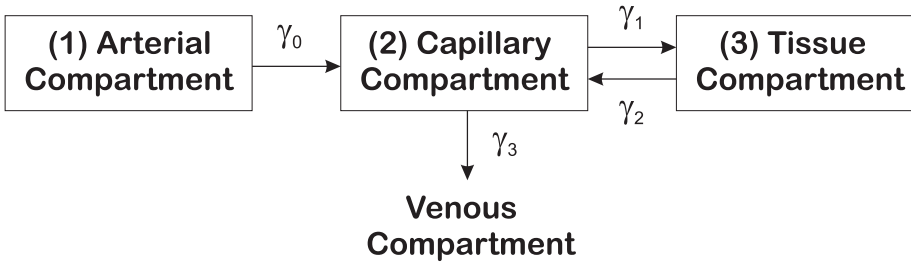

Fig. 2. Movement of oxygen in two vascular and a tissue compartments

rate γ_3 denotes the HbO_2 drainage into the venous compartment. Assuming constant rates, the kinetic equations for the compartment model in Fig. 2 are:

$$\begin{aligned} \dot{f}_1 &= -\gamma_0 f_1, \\ \dot{f}_2 &= \gamma_0 f_1 + \gamma_2 f_3 - (\gamma_1 + \gamma_3) f_2, \\ \dot{f}_3 &= \gamma_0 f_2 - \gamma_2 f_3. \end{aligned} \tag{7}$$

The solution to this linear system of differential equations can be written in a *sum-of-exponentials* model for the ith compartment (see [12], p. 379ff):

$$f_i = k_{i1} \exp(-\gamma_0 t) + k_{i2} \exp(\lambda_0 t) + k_{i3} \exp(\lambda_1 t), \tag{8}$$

where the parameters $\lambda_{0,1}$ and k_{ij} are:

$$\begin{aligned} \lambda_0 &= -\frac{1}{2}\left(\gamma_1 + \gamma_2 + \gamma_3 + \sqrt{(\gamma_1 + \gamma_2 + \gamma_3)^2 - 4\gamma_2\gamma_3}\right), \\ \lambda_1 &= -\frac{1}{2}\left(\gamma_1 + \gamma_2 + \gamma_3 - \sqrt{(\gamma_1 + \gamma_2 + \gamma_3)^2 - 4\gamma_2\gamma_3}\right), \\ k_{1j} &= [1, 0, 0], \\ k_{2j} &= \left[\frac{\gamma_0(\gamma_2 - \gamma_0)}{(\gamma_0 + \lambda_0)(\gamma_0 + \lambda_1)}, \frac{\gamma_0(\gamma_2 + \lambda_0)}{(\gamma_0 + \lambda_0)(\lambda_0 - \lambda_1)}, \frac{\gamma_0(\gamma_2 + \lambda_1)}{(\gamma_0 + \lambda_1)(\lambda_1 - \lambda_0)}\right], \\ k_{3j} &= \left[\frac{\gamma_0\gamma_1(\gamma_2 - \gamma_0)}{(\gamma_0 + \lambda_0)(\gamma_0 + \lambda_1)}, \frac{\gamma_0\gamma_1(\gamma_2 + \lambda_0)}{(\gamma_0 + \lambda_0)(\lambda_0 - \lambda_1)}, \frac{\gamma_0\gamma_1(\gamma_2 + \lambda_1)}{(\gamma_0 + \lambda_1)(\lambda_1 - \lambda_0)}\right]. \end{aligned} \tag{9}$$

The parameter vector $\boldsymbol{\beta}$ for this model consists of 8 items (γ_i: 4 transfer rates, a: gain, t_0: neuronal response onset, t_1: neuronal response duration, b: offset). We attribute a, t_0, and t_1 as "neuronal" parameters, resp. the transfer rates as vascular parameters.

2.2 Stochastic Background Model

It was shown [15,16] that the stochastic part in preprocessed fMRI data may approximately be described by an Ornstein-Uhlenbeck process [17]: (1) it is stationary with respect to time, (2) its elements ϵ_i are normally distributed with

a covariance matrix $\mathbf{V}$ (see 1) and (3) their correlation is described by an AR(1) model. We assume that the spatio-temporal covariance matrix $\mathbf{V}$ is separable in space and time:

$$\mathbf{V} = \mathbf{S} \odot \mathbf{T}, \tag{10}$$

where $\odot$ denotes the Kronecker product. The elements of the (spatial) covariance matrix $\mathbf{S}$ are given by the variance $s_{ii} = \sigma^2$ and the covariance $s_{ij} = cov(h)$ which depend on the distance h of the voxels i and j. Most easily, a semivariogram $\eta(h)$ [18] is used to determine the type of stationary dependence in the data:

$$\eta(h) = \sigma^2 - cov(h) \approx \frac{1}{2 * n_h} \sum_{(i,j) \in N(h)} (y_i - y_j)^2, \tag{11}$$

where $N(h)$ is the set of voxel pairs at distance h, and n_h is the number of pairs in the set. For an AR(1) process with positive correlations, an exponential function fits to the semivariogram:

$$\eta(h) = \alpha_0(1 - \exp(-\alpha_1 h)), \tag{12}$$

where h is the distance between voxel sites. From the model parameters, we can derive the variance $\sigma^2 = \alpha_0$ and the autocorrelation $\rho = \exp(-\alpha_1)$. The covariance matrix $\mathbf{S}$ of a linear array of k voxels is defined as:

$$\mathbf{S} = \sigma^2 \begin{pmatrix} 1 & \rho & \rho^2 & \cdots & \rho^{k-1} \\ \rho & 1 & \rho & \cdots & \rho^{k-2} \\ \rho^2 & \rho & 1 & \cdots & \rho^{k-3} \\ & & & \cdots & \\ \rho^{k-1} & & & \cdots & 1 \end{pmatrix}, \tag{13}$$

Similarly, a matrix $\mathbf{T}$ is formed for the temporal domain and composed as given in 10.

2.3 Estimation

We find the ML estimate $\hat{\boldsymbol{\beta}}$ of our model parameters as the vector $\boldsymbol{\beta}$ that minimizes the quantity:

$$\arg\min_{\beta} \left\{ (\mathbf{y} - g(\mathbf{t}, \boldsymbol{\beta}))^T \mathbf{V}^{-1} (\mathbf{y} - g(\mathbf{t}, \boldsymbol{\beta})) \right\}. \tag{14}$$

In the case of the Gaussian function in model 1, this problem corresponds to a 4-dimensional nonlinear minimization problem, which can easily be solved by the downhill simplex method of Nelder and Mead [19]. This method is not feasible with the more complex models 2 and 3, where the cost function (14) is expected to possess multiple local minima. Because derivatives of the model functions are only available as finite difference approximations, derivative-free optimization methods are preferable. We investigated the use of (1) a combination of simulated annealing with the downhill simplex method [19], (2) Shor's minimization method [20], and (3) an optimization using a genetic algorithm [21].

2.4 Confidence Limits and Statistical Tests

Using a first-order linear model, we can derive confidence limits for the estimation from the inverse of the Fisher information matrix $\mathbf{F}$ [22]:

$$\hat{\boldsymbol{\beta}} \sim N(\boldsymbol{\beta}, \mathbf{F}_{\boldsymbol{\beta}}^{-1}), \quad \text{where} \quad \mathbf{F}_{\boldsymbol{\beta}} = \mathbf{G}_{\boldsymbol{\beta}} \mathbf{V}^{-1} \mathbf{G}_{\boldsymbol{\beta}}^{T}, \tag{15}$$

and $\mathbf{G}_{\boldsymbol{\beta}}$ denotes the Jacobian matrix of $g(\cdot)$ with respect to $\boldsymbol{\beta}$.

A simple measure for the goodness-of-fit (GOF) is given by the χ^2-statistics:

$$\chi^2 = \boldsymbol{\epsilon}^T \mathbf{V}^{-1} \boldsymbol{\epsilon}, \quad \text{where} \quad \boldsymbol{\epsilon} = \mathbf{y} - g(\mathbf{t}, \boldsymbol{\beta}) \tag{16}$$

A more complex measure is derived for the F-statistics, following Hartley [23]:

$$\mathbf{P} = \mathbf{G}_{\boldsymbol{\beta}} \mathbf{F}_{\boldsymbol{\beta}}^{-1} \mathbf{G}_{\boldsymbol{\beta}}^{T} \tag{17}$$

$$F_{p,n-p} \sim \frac{(n-p)}{p} \frac{\boldsymbol{\epsilon}^T \mathbf{P} \boldsymbol{\epsilon}}{\boldsymbol{\epsilon}^T (\mathbf{I}_n - \mathbf{P}) \boldsymbol{\epsilon}}, \tag{18}$$

where n corresponds to the number of data points, p to the number of parameters, and $\mathbf{I}_n$ is the $n * n$ identity matrix.

3 Experiments

To study the usefulness of this modeling approach, we re-evaluated datasets acquired in a fMRI study of working memory [24].

Behavioral Experiment: Subjects learned three sets of letters (4, 6 or 8 characters) at least two days before the scanning session. A trial started with the display of a small red box (for 800ms), followed by the cue and, after a delay (0, 2 or 4 seconds), the probe. Subjects had to indicate by a button press whether the probe item belonged to the cued set. 108 randomized trials were run using an intertrial interval of 18s.

fMRI Parameters: During the behavioral experiment, 7 axial slices (64x64 voxels, 3.8x3.8x5mm voxel size, 2mm gap) were recorded on a Bruker Medspec 300 system using an EPI protocol with a repetition time of 1s. All timings were corrected for the slice acquisition delay in the EPI protocol.

Preprocessing: We randomly selected data obtained from 4 subjects. Data were preprocessed by (1) correction for in-plane movements and (2) corrected for baseline fluctuations, (3) lowpass filtered in the temporal domain to reduce the amount of system and physiological noise (see [25] for details). As a result of this preprocessing, only the fundamental frequency (corresponding to the stimulation) and its first harmonic were retained in the temporal domain of the data.

Definition of ROIs: Standard procedures were applied to detect functional activation in the datasets: (1) analysis for activated regions by Pearson correlation with a time-shifted box-car waveform ($\Delta = 6s$), (2) conversion of the correlation

coefficient into z-scores and thresholding of the corresponding z-map by a score of 10, (3) assessment of the activated regions for their significance on the basis of their spatial extent [26]. Now that we detected voxels with functional activation, we defined ROIs by collecting the 6 most highly activated voxels around local maxima in the z-map. We obtained a total of 94 ROIs from 4 subjects. An illustrative map of ROIs is shown in Fig. 3.

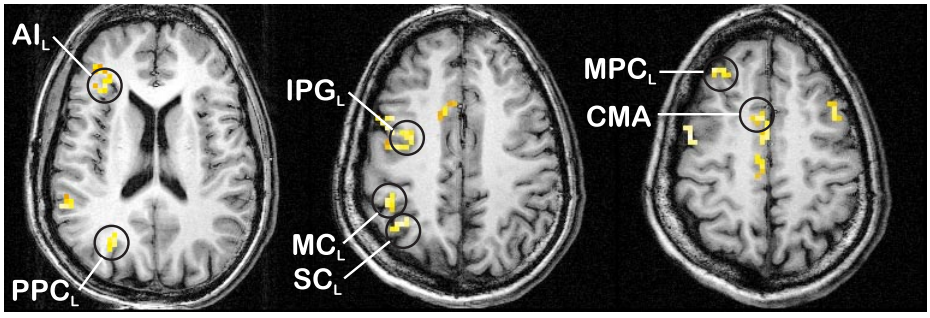

Fig. 3. An illustrative z-map overlay onto the corresponding anatomical from the working memory experiment. Neurofunctionally interesting ROIs are labeled: AI_L: superior anterior insula, MPC_L: middle prefrontal cortex, IPG_L: inferior precentral gyrus, CMA: cingulate motor area, MC_L: motor cortex, PPC_L: posterior parietal cortex, SC_L: sensory cortex

Averaging: To reduce the number of estimations, we averaged voxels within a ROI at a given timestep and across trials with the same delay time manipulation (0, 2, and 4 s). So per ROI, we obtained three different timecourses of 18 timepoints each. As a consequence of averaging in space, we simplified our estimation model by setting $\mathbf{S} = \mathbf{I}_k$, where $k = 6$.

Tests We adapted the 3 HR models defined in the preceeding section to the 3 averaged timecourses in the 94 ROIs. To achieve realistic solutions, we constrained the solution space by the following intervals:

- *model 1:* gain: $0 <= a < 5000$, dispersion: $0 <= d_0 < 10$, lag: $0 <= t_0 < 10$, and baseline: $-500 < b <= 0$,
- *model 2:* onset and duration: $0 <= t_i < 10$, dispersions, gain and offset as above.
- *model 3:* diffusion constants: $0 <= \gamma_i < 10$, onset, duration gain and baseline as above.

For model 1, the downhill simplex algorithm was applied, with computation times of less than a second per estimation. For models 2 and 3, we achieved the best GOFs using the genetic algorithm. Parameters of the genetic optimization process were: 1000 generations, 500 population members, p(exchange) = 0.2, p(mutation) = 0.01, p(crossover) = 0.2.

4 Results

To give an impression of typical waveforms and modeling results, we selected a signal from the left motor cortex MC_L (see Fig. 3) in one of the subjects. Averaged HRs of different experimental delay times are shown in Fig. 4.

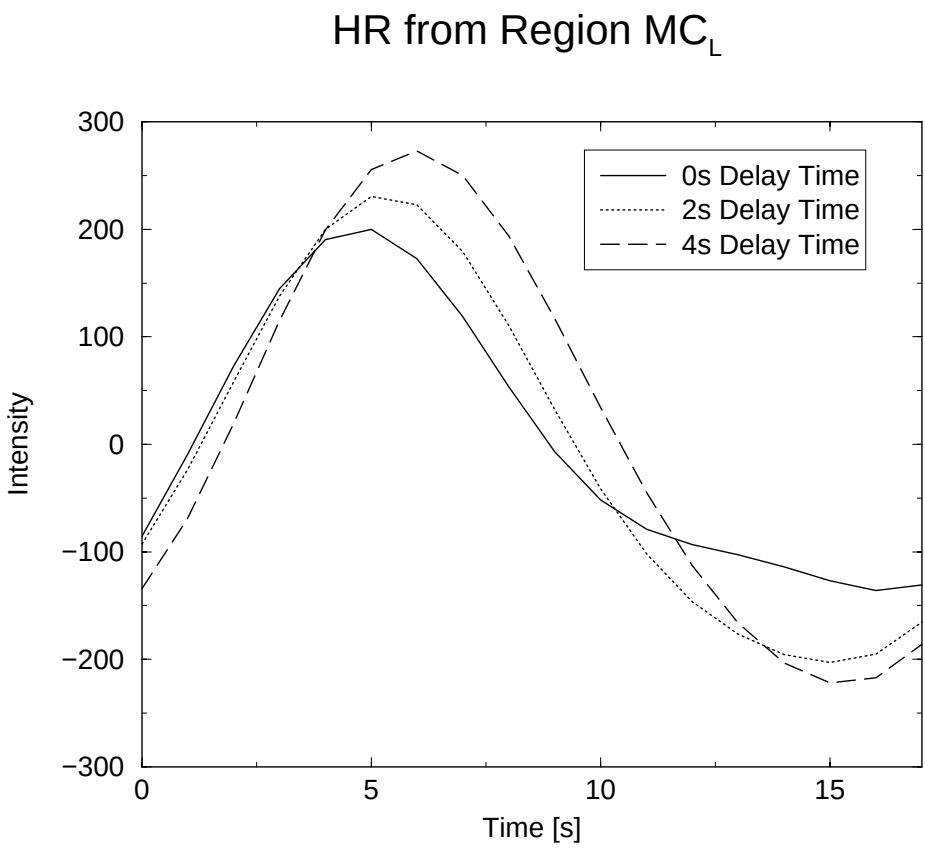

Fig. 4. HRs from region MC_L for the 3 different delay times

For longer delays, the HR in this region was higher, the time-to-maximum and duration were longer. This was reflected in the parameters of the 3 HR models (see Table 1). For all models, the increasing height of the HR with delay time was found as an increase of the gain a. For model 1, the shift of the time-to-maximum led to an increase of t_0, the increasing width to an increase in the dispersion d_0. For model 2, the parameters attributed to the hemodynamic modulation (d_0 and d_1) were relatively independent of the delay time manipulation. Shift and delay were reflected in increasing values of t_0 and t_1. Finally, with the

convolved compartment model, only an increase of t_1 with the delay was found, rate constants were similar.

Table 1. HR parameters for the signals in Fig. 4 for the 3 different experimental delays

Model 1: Gaussian Function

Delay [s]	a	t_0 [s]	d_0 [s]	χ^2
0	324	3.95	2.78	2381
2	429	4.34	3.21	1270
4	496	5.05	3.34	1994

Model 2: Convolved Asymmetric Gaussian Function

Delay [s]	a	t_0 [s]	t_1 [s]	d_0 [s]	d_1 [s]	χ^2
0	2324	2.58	3.31	2.00	3.30	724
2	3420	3.45	3.55	2.94	3.07	1193
4	4062	3.36	5.05	2.78	3.04	1625

Model 3: Convolved Compartment Model

Delay [s]	a	t_0 [s]	t_1 [s]	γ_0	γ_1	γ_2	γ_3	χ^2
0	1847	0.06	5.63	0.66	6.11	4.60	1.27	770
2	2439	0.03	6.47	0.39	6.50	6.10	1.54	1934
4	3056	0.06	7.24	0.60	6.17	6.56	1.52	2161

By inspection of the waveforms, we typically found that ROIs in all subjects showed an increase of the time-to-maximum and the gain with increasing delay time, similar to the example HR in Fig. 4. A closer examination of the estimated modeling parameters by a cluster analysis revealed differences, which allowed us to group ROIs into 4 categories (see Table 2):

- *Group 1*: early rise, little dependence on the delay time manipulation. ROIs of this category were found in cortical areas, which are relevant for encoding the stimulus. Examples include the posterior parietal cortex PPC_L.
- *Group 2*: early rise, delay dependence: ROIs of this category are relevant for maintaining the stimulus. Examples include the anterior insula AI_L.
- *Group 3*: late rise, delay dependence: ROIs take part in the decision process following the delay and for generating the motor response. An ROI in the primary motor cortex (MC_L) belongs to this group.
- *Group 4*: late rise, little delay dependence. An example for this group is given with the sensory cortex (SC_L): subjects left their finger on the response button independent on the delay time.

In accordance with the observation of general delay dependence, most ROIs either belong to group 2 or group 3. It is interesting to note that most early

Table 2. Onset (t_0), duration (t_1) and end time ($t_e = t_0 + t_1$) of the neuronal activation as estimated by model 2. Examples for 4 groups defined by their different temporal behaviour are shown. ROI labels correspond to Fig. 3, all values are given in [s]

	Group 1: PPC_L			Group 2: AI_L			Group 3: MC_L			Group 4: SC_L		
Delay	t_0	t_1	t_e	t_0	t_1	t_e	t_0	t_1	t_e	t_0	t_1	t_e
0	2.90	1.74	4.64	3.27	0.71	3.98	4.02	1.46	5.48	4.04	4.26	8.30
2	2.78	2.54	5.32	2.86	1.85	4.91	3.71	4.68	8.39	4.80	4.34	9.14
4	3.90	1.64	5.54	2.92	3.61	6.53	4.92	4.89	9.81	4.98	4.93	9.91

activated areas in group 2 exhibited their delay time dependence in the duration time t_1, while late responses in group 3 showed a delay time dependence in the end time t_e. This finding may be interpreted as a pre-activation of group 3 areas during the delay phase: i.e. the motor cortex is "held active" until the response decision following the delay period.

Experiences with the 3 models were summarized as:

- *Model 1:* For the Gaussian model, 3 parameters describe the shape of the response: the lag t_0, the dispersion d_0, and the gain a. It was shown [9] that these parameters are interpretable in terms of the experimental stimulation. However, there is no distinction between parameters describing the hemodynamic modulation and neuronal activation in this model. Thus, no decision is possible whether a wide HR is due to a longer activation (i.e. a neuronal effect) or a longer dispersion (i.e. a hemodynamic effect). However, good convergence properties allowed us to use a rather simple and very efficient optimization scheme.
- *Model 2:* Fits are better in comparison with model 1, often down to $\chi^2 \approx 50$, which was a consequence of modeling the HR asymmetry by two different dispersion parameters. As it was suspected previously [9], HRs which arise early and follow short stimuli were found asymmetric with a shorter rising edge d_0 (typically 2-3s) than falling edge d_1 (typically 3-4s). Late and wide HRs tend to be symmetric with dispersions in the order of 3-4s. The attributed neuronal activation parameters, onset t_0, and duration t_1, are interpretable in the context of the fMRI experiment. A genetic algorithm was necessary to optimize this model, so there is a marked increase in the computation time (12min per estimation) in comparison with the previous model.
- *Model 3:* We adapted HRs both to model equations for the capillary compartment 2 and the tissue compartment 3. Fits for both compartments are comparable with model 1, with slightly better values for compartment 2. This is in agreement with the mechanism of the BOLD effect; the fMRI signal arises from the vascular compartment. Rates γ_0 (inflow) and γ_3 (outflow) (see Fig. 2) were found between 0.3-0.7, rates γ_1 (vessel to tissue) and γ_2 (tissue to vessel) in the order of 6-9. This is interpretable as an easy transfer

(of oxygen) between the vascular and tissue compartment, while the sluggish (active) effect of vascular dilatation and constriction was modeled by low inflow and outflow rates. Onset times t_0 were always below 1s, and the duration in the order of 4-7s. With the current formulation and optimization approach, this model needs the rather high amount of computation time of 32min per waveform.

5 Discussion

The description of the HR by a model function is considered as an advantage because it provides a compact and concise parameterization of the HR shape. Current choices for model function are arbitrary, since none is based on a comprehensive physiological model. Our preference for the Gaussian function in previous studies was only justified by the fact that we observed the best fits in a non-linear estimation procedure.

In this study we tested the feasibility of separating "neuronal" from "vascular" parameters by introducing complex HR model functions. Separating hemodynamic from neuronal factors is highly desirable in cognitive research, not only to better characterize the neuronal mechanisms of a cognitive task, but also to better understand the reasons for interindividual differences in terms of "good" and "bad" responders in fMRI experiments.

From experiences with model 2 we confirmed that asymmetries are present in HRs. By including parameters to adapt to asymmetries, marked improvements in the fits were achieved, especially with brief stimuli and early responses. The introduction of the convolution operation in the modeling context allowed us to separate parameters. However, no experimental justification yet exists for the designation as neuronal or vascular properties other than the conformance of results with the current understanding of cognitive processes involved in the example fMRI study. However, it is rather easy to design fMRI experiments better targeted towards a justification of this hypothesis.

The non-linear regression model from (1) and (14) allows the use of complex, highly non-linear functions in our problem domain. We had to resort to a costly optimization method (the genetic algorithm) and to averaged waveforms instead of using single trial data directly. From this feasibility study we learned that it is possible to derive rather narrow limits for hemodynamic modulation parameters.

An interesting reformulation of the compartment model follows from the observation that oxygen delivery to the tissue compartment obeys a Hill-type equation [11,27], i.e. transfer rates γ_i from the vascular to the tissue compartment are non-linear functions of the oxygen tension. At least in healthy subjects, this functional dependency is well described and thus may be introduced in a more complex formulation of the compartment model in 7. Since usually only a few timesteps per trial are recorded, there is an upper bound for the parameter number for any model function.

We regard HR modeling as a new tool in fMRI data analysis which will lead to a deeper understanding of the mechanisms underlying the physiological

and neuronal basis of brain functioning. Models as proposed in this paper open another approach for investigating the dynamical properties of the brain.

References

1. Belliveau, J.W., Kennedy, D.N., McKinstry, R.C., Buchbinder, B.R., Weisskoff, R.M., Cohen, M.S., Vevea, J.M., Brady, T.J., Rosen, B.R.: Functional mapping of the human visual cortex by magnetic resonance imaging. Science **254** (1991) 716-719
2. Vilringer, A., Dirnagl, U.: Coupling of brain activity and cerebral blood flow: basis of functional neuroimaging. Cerebrovascular and Brain Metabolism Review **7** (1995) 240-276
3. Friston, K.J., Holmes, A.P., Worsley, K.J., Poline, J.B., Williams, C.R., Frackowiak, R.S.J.: Analysis of functional MRI time-series. Human Brain Mapping **1** (1994) 153-171
4. Kim, S.G., Richter, W., Ugurbil, K.: Limitations of temporal resolution in functional MRI. Magnetic Resonance in Medicine **37** (1997) 631-636
5. Lange, N., Zeger, S.L.: Nonlinear Fourier time series analysis for human brain mapping by functional magnetic resonance imaging. Journal of the Royal Statistical Society: Applied Statistics **46** (1997) 1-29
6. Cohen, M.S.: Parametric analysis of fMRI data using linear systems methods. Neuroimage **6** (1997) 93-103
7. Friston, K.J., Josephs, O., Rees, G., Turner, R.: Nonlinear event-related responses in fMRI. Magnetic Resonance in Medicine **39** (1998) 41-52
8. Rajapakse, J.C., Kruggel, F., von Cramon, D.Y.: Modeling hemodynamic response for analysis of functional MRI time-series. Human Brain Mapping **6** (1998) 283-300
9. Kruggel, F., von Cramon, D.Y.: Modeling the hemodynamic response in single trial fMRI experiments. Magnetic Resonance in Medicine (in press)
10. Buckner, R.L., Koutstaal, W., Schacter, D.L., Dale, A.M., Rotte, R., Rosen, B.R.: Functional-anatomic study of episodic retrieval using fMRI (II). Neuroimage **7** (1998) 163-175
11. Gjedde, A.: The relation between brain function and cerebral blood flow and metabolism. In: Cerebrovascular disease. Lippincott-Raven, Philadelphia (1997)
12. Seber, G.A.F., Wild, C.G.: Nonlinear Regression. Wiley, New York (1989)
13. Widmark, E.M.P.: Studies in the concentration of indifferent narcotics in blood and tissues. Acta Medica Scandinavia **52** (1920) 87-164
14. Rescigno, A., Lambrecht, R.M., Duncan, C.C.: Mathematical models in the formulation of pharmacokinetic models. Lecture Notes in Biomathematics Vol. 48, Springer, Heidelberg (1983) 59-119
15. Bullmore, E., Brammer, M., Williams, S.C.R., Rabe-Hesketh, S., Janoth, N., David, A., Mellers, J., Howard, R., Sham, P.: Statistical methods of estimation and inference for functional MR image analysis. Magnetic Resonance in Medicine **35** (1996) 261-277
16. Benali, H., Buvat, I., Anton, J.L., Pelegrini, M., Di Paola, M., Bittoun, J., Burnod, Y., Di Paola, R.: Space-time statistical model for functional MRI image sequences. In: Information Processing in Medical Imaging (LCNS 1230). Springer, Heidelberg (1997) 285-298
17. Neumaier, A., Schneider, T.: Multivariate autoregressive and Ornstein-Uhlenbeck processes: estimates for order, parameters, spectral information, and confidence regions. ACM Transactions in Mathematical Software (in press)

18. Cressie, N.A.C.: Statistics for spatial data. Wiley, New York (1993)
19. Press, W.H., Flannery, B.P., Teukolsky, S.A., Vetterling, W.T.: Numerical recipes in C. Cambridge University Press, Cambridge (1992)
20. Shor, N.Z.: Minimization methods for nondifferentiable optimization. Springer Series in Computational Mathematics, Vol. 3. Springer, Heidelberg (1985)
21. Goldberg, G.E.: Genetic algorithms in search, optimization, and machine learning. Addison-Wesley, Reading (1989)
22. Cox, C., Ma, G.: Asymptotic confidence bands for generalized nonlinear regression models. Biometrics **51** (1995) 142-150
23. Hartley, H.O.: Exact confidence regions for the parameters in nonlinear regression laws. Biometrika **51** (1964) 347-353
24. Zysset, S., Pollmann, S., von Cramon, D.Y., Wiggins, C.J.: Retrieval from long term memory and working memory. In: Cognitive Neuroscience Society: 1998 Annual Meeting Abstract Program, MIT Press, Harvard (1998) 83
25. Kruggel, F., Descombes, X., von Cramon, D.Y.: Preprocessing of fMR datasets. In: Workshop on Biomedical Image Analysis (Santa Barbara), IEEE Computer Press, Los Alamitos (1998) 211-219
26. Friston, K.J., Worsley, K.J., Frackowiak, R.S.J., Mazziotta, J.C., Evans, A.C.: Assessing the significance of focal activations using their spatial extent. Human Brain Mapping **1** (1994) 210-220
27. Gjedde, A., Poulsen, P.H., Østergard, L.: Model of oxygen delivery predicts deoxygenation of hemoglobin. Neuroimage **7** (1998) S248